

HI AND OH ABSORPTION TOWARD NGC 6240

Willem A. Baan

ASTRON, Westerbork Observatory,¹ P.O. Box 2, 7990 AA Dwingeloo, The Netherlands

baan@astron.nl

Yoshiaki Hagiwara

National Astronomical Observatory of Japan, 2-21-1 Osawa, Mitaka, Tokyo, Japan

yoshiaki.hagiwara@nao.ac.jp

Peter Hofner

Physics Department, New Mexico Tech, Socorro, NM 87801

and

National Radio Astronomy Observatory,² P.O. Box O, Socorro, NM 87801

phofner@nrao.edu

ABSTRACT

VLA observations of large-scale HI and OH absorption in the merging galaxy of NGC 6240 are presented with 1 arcsec resolution. HI absorption is found across large areas of the extended radio continuum structure with a strong concentration towards the double-nucleus. The OH absorption is confined to the nuclear region. The HI and OH observations identify fractions of the gas disks of the two galaxies and confirm the presence of central gas accumulation between the nuclei. The data clearly identify the nucleus of the southern galaxy as the origin of the symmetric superwind outflow and also reveal blue-shifted components resulting from a nuclear starburst. Various absorption components are associated with large-scale dynamics of the system including a foreground dust lane crossing the radio structure in the northwest region.

Subject headings: galaxies: ISM — galaxies: nuclei — ISM: molecules — masers — galaxies: starburst

1. Introduction

The chaotic appearance of NGC 6240 at all wavelengths is due to a forceful galactic collision of two galaxies (Fosbury & Wall 1979). The two individual nuclei of NGC 6240 were first detected in R and I bands at a projected distance of 1.8" or 0.9 kpc (Fried & Schulz 1983). Early H α studies revealed extended emission with two independent and almost perpendicular disk systems (Bland-Hawthorn et al. 1991).

NGC 6240 is a prototypical Luminous Infrared Galaxy with an IR luminosity of $L_{IR} = L_{8-1000\mu m} = 6 \times 10^{11} L_{\odot}$ (Sanders et al. 1988). The FIR luminosity of these galaxies is powered by extremely high star-formation activity and or an embedded AGN. For NGC 6240 the mid-IR observations are consistent with a dominant starburst power contribution of approximately 75% within the central 5 kpc (Genzel et al. 1998).

Radio data show two nuclei embedded in a connecting structure that extends into a loop structure to the West (Condon et al. 1982; Colbert et al. 1994) also seen in our continuum data (see Figure 1). MERLIN and the Very Long Baseline Array (VLBA) observations of the two nuclear continuum sources show brightness temperatures of 7×10^6 K for the northern component and 1.8×10^7 K for the southern component (Gallimore & Beswick 2004). The inverted spectra at low frequency confirm the AGN nature at each of the nuclei. The loop results most likely from a bubble front swept up by a superwind emanating mostly from the southern nucleus (designated as N1 in Figure 1)(Colbert et al. 1994; Ohyama et al 2000). NGC 6240 exhibits HI and OH absorption against the nuclear continuum (Baan et al. 1985). Recent HI absorption studies at 0.3 arcsecond resolution with MERLIN distinguish the absorption at each of the two nuclear components (Beswick et al. 2001).

ASCA, XMM and Chandra data confirm the presence of two deeply buried AGNs in the NGC 6240 system on the basis of a hard X-ray component with neutral Fe K α lines in addition to the soft X-ray components due to the starburst (Iwasawa & Comastri 1998; Boller et al. 2003; Komossa et al. 2003). The most prominent AGN is located at the southern nucleus N1, where the obscuration is the highest. The extended X-ray emission has a close correlation with the well-known (butterfly-shaped) H α emission. H α studies with HST confirm the presence of filamentary structures filling the inner volume of the arc and confirm the presence of confining walls of the outflow at either side of the nucleus (Gerssen

¹The Westerbork Observatory is part of the Netherlands Foundation for Research in Astronomy (NFRA-ASTRON) and is partially funded by the Organization for Scientific Research (NWO) of The Netherlands.

²The National Radio Astronomy Observatory is a facility of the National Science Foundation operated under cooperative agreement by Associated Universities, Inc.

et al. 2004). Significant $H\alpha$ structures have also been found in NGC 6240 in the form of a butterfly-shaped structure that partially superposes the radio arc and extended radio structure.

NGC 6240 displays strong H_2 $v = 1-0$ S(1) and [Fe II] line emission that peaks between the stellar light of the nuclei but lies closer to the southern nucleus (van der Werf et al. 1993; Joseph & Wright 1985; Ohyama et al. 2000). Spectroscopic studies of H_2 at K band allow the separation of the dynamics of the two nuclei (Tecza et al. 2000). The NIR light of each of the nuclei is dominated by red super-giants formed during a short episode of intense star-formation 15-25 million years ago. K band infrared imaging with Keck II and NICMOS on the Hubble Space Telescope has revealed elongated structures at both the North and South nuclei and considerable substructure within each nucleus (Max et al. 2005). Additional point-like regions are found around the two nuclei, which are thought to be young super-star-clusters.

CO(2–1) emission studies with the IRAM interferometer show a similar structure as the H_2 emission and also peaks between the two nuclei (Tacconi et al 1999). Most of the CO flux is concentrated in a thick and turbulent disk-like structure between the two IR/radio nuclei. Studies with Nobeyama Rainbow interferometer (Hagiwara 1998) indicate that the HCN(1-0) and HCO^+ fluxes also peak between the nuclei, and do not coincide with the star-forming region in the galaxy (Nakanishi et al. 2005). The molecular structure accounts for a large fraction (30-70%) of the dynamic mass. Although the central location of the molecular material in NGC 6240 is not unique, it is notably different from the (more advanced) interaction in Arp 220 where the emission peaks at the two nuclei (Scoville et al 1997; Sakamoto et al 1999).

This paper presents studies of the OH and HI absorption in the NGC 6240 system using the NRAO Very Large Array (VLA) in A-Configuration. With NGC 6240 at a distance of 104 Mpc the spatial conversion for the VLA data is 504 pc per arcsecond, which complements the resolution of other spectral line and continuum studies. Our data reveal more of the dynamics of the system and provide connections to studies of other atomic and molecular emissions.

2. Observations

Observations of the HI 21 cm line and the OH main lines at 1665 and 1667 MHz toward NGC 6240 were made on September 1, 1995 with the NRAO Very Large Array in the A-configuration. Phase tracking was centered on $\alpha(1950) = 16^h50^m28^s.3$, $\delta(1950) = 02^\circ28'53''$.

The HI line was observed using a 2 IF mode, each IF having a bandwidth of 6.25 MHz subdivided into 32 channels of 195.3 kHz in width. This setup resulted in a usable velocity coverage of 1298 km s^{-1} and a velocity resolution of 43.3 km s^{-1} . The spatial resolution in the HI spectral data is $1.95'' \times 1.79''$ for NA weighting and the channel width is 43.3 km s^{-1} . The rms in the individual channel maps is $0.49 \text{ mJy beam}^{-1}$.

Both OH lines at 1665 and 1667 MHz were observed simultaneously using two partially overlapping IFs of width 6.25 MHz with 32 channels of width 195.3 kHz. The synthesized band used for this discussion has a center frequency of 1666.38 MHz (between those of the 1665 and 1667 MHz lines) and has a total velocity coverage of 1326 km s^{-1} . The velocity scale in this presentation is heliocentric in the optical definition and has been re-gridded using the rest frequency of the 1667 MHz line. The resolution in the OH maps is $1.11 \times 1.08''$ and the channel width is 36.7 km s^{-1} . The rms in the channel maps is $0.41 \text{ mJy beam}^{-1}$.

Continuum maps at 21 and 18-cm have been constructed using line-free channels. The rms and the beam size of the two maps are respectively $0.46 \text{ mJy beam}^{-1}$ with $1.965'' \times 1.79''$ and $0.28 \text{ mJy beam}^{-1}$ with $1.11'' \times 1.08''$.

The data were reduced using the NRAO software package AIPS. The flux and bandpass calibrator and phase calibrator were 3C 286 and 1648+015 for both HI and OH line data sets. Image cubes were made with a pixel size of $0''.3$, using a variety of weighting schemes. Continuum data sets were constructed by averaging line-free channels. Subtraction of the continuum was done independently in the visibility and in the image domain, resulting in consistent results. In the case of the OH data both IFs were imaged independently and joined after the continuum subtraction, averaging overlapping channels. Due to the uncertainty of the baseline structure at the edges of the spectrum, we estimate a flux uncertainty of 20% for the OH absorption data and 10% for the HI absorption and the continuum data.

3. Results

The distance of NGC 6240 is assumed to be $D = 104 \text{ Mpc}$ for a systemic optical velocity of 7275 km s^{-1} using $H_0 = 70 \text{ km s}^{-1} \text{ Mpc}^{-1}$. At this distance the spatial conversion is 504 pc per arcsecond. In the discussions below, we have adopted the radio designations of Colbert et al. (1994) for the nuclei N1 and N2 and the components of NGC 6240. In addition, the suggestion has been made for the northern component N3, which may be a third nucleus or an enhanced fragment of the northern galaxy. There is a Southern extension S and various West components W1 - W4 forming the arc structure of 5.9 kpc in size. A W0 component has been designated in the continuum structure to the west of N3. These designations have

been indicated in Figure 1b.

3.1. Continuum studies

Contour maps of the natural-weighted continuum emission at 1420 MHz and the robust-weighted continuum emission at 1666 MHz are presented in Figure 1. The integrated flux densities in the maps are 466 and 333 mJy with peak values 108 and 58 mJy, respectively. Our A-array L-band images are consistent with previous B-array images except that our peak fluxes are higher by 10–20%, when convolved to a resolution of $4.79'' \times 4.39''$ of Colbert et al. (1994), possibly due to slightly different integration boxes. The 21 cm map shown in Figure 1a (upper panel) is optimized for the detection of extended low-brightness features and shows that the individual radio components N1 (South) and N2 (+N3) (North) are embedded in a halo of diffuse emission. The higher resolution 18 cm map in Figure 1b (lower panel) clearly separates the two nuclei N1 and N2 (+N3). At higher resolution the N1–N2 axis is found to be at $PA = 20^\circ$ with a (projected) separation of the nuclei of $1.575''$ or 93 pc (Hagiwara et al. 2003; Gallimore & Beswick 2004).

The structure along the western arm (W1–W4) shows diffuse emission without any sharp peaks at this resolution. The new components NW and W0 have been added to indicate the diffuse structure west of N3. Diffuse extensions can be seen in the north-east NE, the south-east SE, and an S extension. We present radio continuum parameters derived from the 1666 MHz map in Table 1.

The large-scale continuum structure shows a strong similarity to the butterfly structure found in the optical and X-ray (Komossa et al. 2003). The primary cause of this structure would be a nuclear blowout from the nuclear region of N1 in the southern galaxy. The large-scale $H\alpha$ structure towards the west (see Max et al. 2005) appears to match and complement the loop structure in the radio. In addition, there eastern complement to the western loop in $H\alpha$ and soft X-ray (Max et al. 2005; Komossa et al. 2003). The SE and NE radio extensions agree with X-ray and $H\alpha$ structure and form "the base" of a similar blowout bubble to the east of the nuclei. The S and NW radio extensions in Figure 1a,b have counterparts also in the larger scale $H\alpha$, H_2 and X-ray emission structures.

3.2. The HI Absorption

The HI line characteristics - The HI absorption spectra in the extended emission region of NGC 6240 have been given in Figure 2. The profiles of the HI absorption at the

two nuclei are very similar as both spectra have a FWZI width of about 900 km s^{-1} and a half-power width of about 348 km s^{-1} . However, the absorption at N2 is 1.7 times stronger than the absorption at N1, and the line at N2 is more symmetric than the N1 line that is skewed due to a higher velocity component. The systemic velocities at N1 and N2 are 7295 km s^{-1} and 7339 km s^{-1} respectively. N1 lies just south of the peak in the HI absorption column density in Figure 2.

The spectra presented in Figure 2 indicate that there are large differences in the absorption columns and that absorption is seen over a velocity range of more than 900 km s^{-1} . This velocity width results from the rotation in each of the galaxies, the orbital velocity component of the two galaxies, and the inflow and outflow due to the interaction. The line of sight to each nucleus does not provide an accurate estimate of the systemic velocity of that nucleus. The spatial resolution of the 21-cm data is $980 \times 900 \text{ pc}$ and our line-of-sight towards the two nuclei will sample multiple velocity components. The high-resolution HI absorption study with MERLIN at 0.3 arcsec resolution by Beswick et al. (2001) revealed two isolated absorption components at the locations of the N1 and N2 nuclei at velocities 7087 and 7260 km s^{-1} (radio definition). Using the optical heliocentric definition we find systemic velocities $V(\text{N1}) = 7258 \text{ km s}^{-1}$ and $V(\text{N2}) = 7440 \text{ km s}^{-1}$ and we adopt these as a more accurate approximation of the systemic velocities of the two nuclei. It should be noted that these velocities straddle the absorption peak in the two nuclear absorption spectra of Figure 2. While the peak of the absorption column density coincides with N1, the centroid absorption velocity at N1 is about 100 km s^{-1} lower, due to the lower velocity of the structural component between the nuclei.

The HI PV diagrams - Figures 3 and 4 present velocity-position maps in two principal E-W and N-S directions. These diagrams cover only the double-nucleus region. The RA–velocity diagrams of Figure 3 show the velocity structure in the south and the north of the system. Close to N1 where the column density peaks at 7265 km s^{-1} , the rotation is essentially south-to-north with a gradient to be determined from the PV plot along the declination axis. In the northern PV diagram, the extended absorption peaks just south of N2 at 7385 km s^{-1} and shows an west-to-east velocity gradient of $1.0 \text{ km s}^{-1} \text{ pc}^{-1}$ close to N2. In the North, an additional (weak) second component appears at 7700 km s^{-1} with a east-to-west velocity gradient of $0.53 \text{ km s}^{-1} \text{ pc}^{-1}$. The extended low-declination outflow structure south of N1 reaches 6900 km s^{-1} (Fig. 3b) and has a southwest-to-northeast gradient of $0.89 \text{ km s}^{-1} \text{ pc}^{-1}$.

The declination–velocity diagrams of Figure 4 display three velocity profiles along the east side, close to the center, and the west side of the central region (along a south-north RA direction). The diagrams show a changing south-to-north velocity gradient resulting from

three distinct components. South of N1 there is a gradient of $1.49 \text{ km s}^{-1}\text{pc}^{-1}$; north of N2, a gradient of $1.15 \text{ km s}^{-1}\text{pc}^{-1}$. In between N1 and N2 the gradient is $0.26 \text{ km s}^{-1}\text{pc}^{-1}$, which is close to the predicted value of $0.24 \text{ km s}^{-1}\text{pc}^{-1}$ based on the velocity difference of the two nuclei. This central component is dominated by an accumulation of gas in between the two nuclei. A similar absorption structure is found in the OH data. In accordance with Fig. 3, an east-to-west component enters between 7300 and 7750 km s^{-1} , which occurs at high declination at the west side (right frame) of the source, i.e. going towards the NW region and possibly representing streaming gas motions in the northern galaxy. A number of rather marginal but distinctly offset components are found west of N2 (Fig. 4a) and southeast of N2 (Fig. 3a), covering a large velocity range of $7000\text{--}7750 \text{ km s}^{-1}$.

In our discussion of the OH absorption data below, we will correlate our findings of the HI absorption in the nuclear N1–N2 region. However, the OH absorption is solely confined to the nuclear region and does not display any of the extensions found in this section.

The combined PV diagrams show the existence of five independent HI components found against the nuclear region: (1) a disk-like structure with three components with distinct gradients of $1.49 \text{ km s}^{-1}\text{pc}^{-1}$ south of N1, of $1.15 \text{ km s}^{-1}\text{pc}^{-1}$ north of N2, and of $0.26 \text{ km s}^{-1}\text{pc}^{-1}$ between N1 and N2. A single gradient covering the whole range would have a south-to-north gradient of $0.32 \text{ km s}^{-1}\text{pc}^{-1}$.; (2) the region north of N2 shows a second (reverse) southwest-to-northeast gradient of $1.0 \text{ km s}^{-1}\text{pc}^{-1}$; (3) a high-declination east-to-west structure between 7250 and 7750 km s^{-1} with a gradient of $0.53 \text{ km s}^{-1}\text{pc}^{-1}$ providing a connection with the NW absorption region; (4) an outflow component reaching 6900 km s^{-1} associated with nucleus N1 with a southwest-to-northeast gradient of $0.89 \text{ km s}^{-1}\text{pc}^{-1}$; and (5) some distinct (but marginal) offset components covering $7000\text{--}7750 \text{ km s}^{-1}$ associated with the disturbed region west-south-west of the nucleus N1.

The moment maps - The first moment HI map in Figure 5a confirms the dominant south-to-north (component (1)) velocity gradient along the N1 - N2 axis suggesting organized rotation. The velocity gradient deduced between N1 and N2 is $0.18 \text{ km s}^{-1}\text{pc}^{-1}$, which is smaller than the one obtained above from the PV diagrams.

A large-scale east-to-west rotation (component (3)) in the northern region causes curved iso-velocity lines and continues into the NW region but is interrupted by a lower-velocity north-south component crossing the region at W0. This interruption has the signature of the foreground dust lane passing just west of the nuclei in optical images. The dust lane absorption at W0 is at 7400 km s^{-1} , which is close to the systemic velocity of N2.

At the locations of the two nuclei, the systemic velocities in Figure 5a are $V(\text{N1}) = 7235 \text{ km s}^{-1}$ and $V(\text{N2}) = 7305 \text{ km s}^{-1}$. The velocity difference of 70 km s^{-1} is smaller than the

120 km s⁻¹ found in the PV diagrams of Fig. 3, which would come closer to the difference of 182 km s⁻¹ found at higher resolution (Beswick et al. 2002) and in other molecular data. Outside the main structure we can also identify absorption at W2 at $V = 7034$ km s⁻¹ and at the eastern edge of W4 at 7687 km s⁻¹, which needs confirmation.

The second moment map in Figure 5b shows a rather curious structure with a band of large velocity widths (more than 150 km s⁻¹) running from N1 and N2 into the NW region. For comparison, the MERLIN line widths are largest at N2 with 300 km/s and narrowest towards the northwest with 60 km s⁻¹ (Beswick et al. 2001).

A distinct low-velocity component (seen also as 4 and 5 in the PV data) located at west-south-west of N1 is likely related to the superwind outflow. This feature at PA = 25° appears to have an west-to-east velocity gradient and lower line widths. It should be noted that this structure also appears at the same location in the OH data. Furthermore, the position angle of the outflow component also points to the eastern edge of the W4 component that is also found in the moment maps of Fig. 5 and 6. In addition, the offset components found at the outflow position in the PV diagrams have a velocity range of 7000–7750 km s⁻¹, indicating a highly disturbed region.

The HI absorption column density - The absorption column density presented in Figure 6 and in Table 2 is determined using the absorption line strengths and the associated continuum data at 1420 MHz (Figure 1a). The expression for the hydrogen column density used is $N_{\text{H}}/T_{\text{S}} = 1.823 \times 10^{18} \int \tau(V) dV \text{ cm}^{-2}$, where T_{S} is the hydrogen spin temperature, and τ is the absorption optical depth. The map shows the highest column density of $N_{\text{H}} = 1.28 \times 10^{22} \text{ cm}^2$ at nucleus N1 using a spin temperature of 100 K. The optical depth is largest at N1 with 0.15 (± 0.001) and at N2 with 0.11 (± 0.001).

The column density map also shows absorption at W0 with $9.42 \times 10^{21} \text{ cm}^2$, and at W4 with $7.78 \times 10^{21} \text{ cm}^2$. If one assumes that the absorption at W0 is composed of a continuation of the NW absorption plus a contribution of the foreground dust-lane at a significantly lower velocity, then the dust-lane specific column density is estimated at $3.2 \times 10^{21} \text{ cm}^{-2}$. The NW structure at PA = -60° is located at some 2 kpc from the nuclei and W0 is at 2.7 kpc. In addition, the NE elongation at PA = 45° extends almost 2.0 kpc from N2. The absorption spot W4 is 4.2 kpc away from N1.

3.3. The OH Lines

The OH line characteristics - The integrated spectrum of the 1667 MHz and 1665 MHz OH absorption is depicted in Figure 7 in the rest frame of the 1667 MHz line. The

adopted systemic velocities of the two nuclei of 7258 and 7440 km s⁻¹ lie just below and above the absorption peaks of the two lines. The integrated OH spectrum across the whole source shows an overall line ratio of 1.3 for the two absorbing transitions. Channel maps of the OH data cube have not been displayed because the spectral information is better presented by other means.

The shallowness and irregularity of the single-dish OH absorption spectrum (Baan et al. 1985) suggested that some of the absorption in the system had been filled in with emission. With this in mind, the OH data have been scrutinized in a search for OH emission but no clear evidence has been found. The two absorption lines in Fig. 7 suggest an asymmetry of the line profiles and non-similarity that could indeed be explained by a partial infilling with emission on the high velocity side of the 1665 MHz line and/or at the low side of the 1667 MHz line.

The OH hyperfine ratio in the nuclear absorption region is depicted in Figure 8 using the sums of the channel maps for the 1667 and 1665 MHz lines as depicted in Figure 7. The central region between the nuclei exhibits values below 1.0 and going below 0.8 on the west side. Locations outside the central region have values in the optically-thick and optically-thin LTE range of 1.0–1.8. The values of the hyperfine ratios at N1 and N2 are respectively 1.6 and 1.2. The occurrence of non-LTE conditions in the velocity range of 7330 km s⁻¹ and below may be explained with emission in the 1667 MHz line. The range around 7300 km s⁻¹ corresponds to a missing (low-velocity) shoulder of the 1667 MHz line profile (see Fig. 7).

The OH PV maps - The OH data shows substantial absorption only against the nuclear radio double source and no large extensions can be found outside the nuclear area. A single OH velocity-position map is presented at PA = 20° along the N1–N2 axis (Fig. 9). Different than that of the HI absorption, the bulk of the OH absorption occurs between the two nuclear sources at 7325 km s⁻¹, and shows a dominant south-to-north velocity gradient in the central region of 0.19 km s⁻¹ pc⁻¹, which is somewhat smaller than that of the central HI component. Similar to the HI absorption, there is a changing velocity gradient across the region with two separate components with velocity gradients outside N1 and N2. The gradients in the two shoulders in Fig. 9 south of N1 and north of N2 are estimated to be 0.75 km s⁻¹ pc⁻¹, which is much steeper than the central part but still lower than that of the HI estimate. This component has also a counterpart in the 1665 MHz lines and is related to the connecting bridge between the 1665 and 1667 MHz lines.

In the northern region close to N2, there is a distinct component with an (estimated) opposite west-to-east velocity gradient of 0.30 km s⁻¹ pc⁻¹. A similar structure has been found in the HI data (Fig. 4), which has been associated with rotation due to the northern galaxy along the N2–NW line. In the spectrum of Figure 7 this translates into the low-

velocity shoulder of the 1667 MHz line.

The moment maps - The first moment map of the 1667 MHz line in Figure 10a shows a smooth velocity gradient, that resembles and confirms the HI characteristics in the central region. The velocity gradient starts in the SE region close to N1 as part of the southern galaxy and continues via N2 into the northeast direction. There is some evidence of a superposed east-to-northwest gradient starting at N2 that is associated with the northern galaxy. The velocities derived for N1 and N2 from the second moment map are 7255 and 7370 km s⁻¹.

The line width in the 1667 MHz line displayed in Figure 10b is largest at a location between the two nuclei similar to the HI case, but with a value of 80+ km s⁻¹ it is significantly smaller than the 150+ km s⁻¹ width found in HI. It should be noted that the highest line widths coincide partially with the region of non-LTE (super optically-thin with ratio ≤ 1.0) excitation in Figure 8. The moment maps of the 1665 MHz lines are all consistent with those of the 1667 MHz.

Figures 10 also display the curious structure southwest of N1 at PA = -25° that is also present in the HI data, and represents the direction of a jet or is part of a wider nuclear outflow. At that location the velocity field is confused and the OH linewidths become narrower. Further to the west there is an additional (disjoint) region with of very low 20 km s⁻¹ linewidth at 7360 km s⁻¹, which may relate to the (streaked) extensions at low declination (57.0") in the PV diagram (Fig. 9).

The OH column density - The OH column density has been presented in Figure 11 and has been based on the 1667 MHz optical depth using the 18 cm continuum map (Fig. 1) and the expression $N_{\text{OH}67} = 2.35 \times 10^{14} T_{ex} \int \tau(V) dV$, where the excitation temperature T_{ex} has a typical value of 20 K. The region with the highest OH column density of $N_{\text{OH}67} = 1.08 \times 10^{16} \text{ cm}^{-2}$ occurs halfway between N1 and N2. The column densities at N1 and N2 are a factor of about 1.8 lower. The peak OH optical depth of 0.063 is a factor of 2 smaller than that of HI.

4. Discussion

4.1. The central gas concentration

The central gas concentration is clearly present in the OH data, where it peaks between the nuclei at about 0.9" north of N1 (and closer to N2), and also in the HI data, where the peak occurs close to N1. In a projection scenario with N1 being located behind N2 (see

section below), the largest column densities should occur at N1 and gas distributions of the two galaxies are displaced by only 790 pc. Therefore, the column differences between the absorption peaks and the nuclei of 1.3 for HI and 1.8 for OH could be accommodated by a superposition of two galactic gas distributions. However, the velocity gradient in the central region of $0.19 \text{ km s}^{-1}\text{pc}^{-1}$ for OH and $0.26 \text{ km s}^{-1}\text{pc}^{-1}$ for HI is close to the predicted value of $0.24 \text{ km s}^{-1}\text{pc}^{-1}$, that results from the velocity difference of the two nuclei. The central molecular structure is also not tied simply to the orbital motion of the two nuclei, because the emission peak lies off the N1-N2 connecting line. The central gas structure could thus be a superposition of disk gas, which is combined with gas pulled out of the two galaxies during the interaction and deposited close to the center of mass of the system. The structure appears co-rotating within the two nuclear regions.

The centrally peaked OH absorption shows rough agreement with the findings for other thermally excited molecules such as the CO $J = 2-1$ and H_2 emissions (van der Werf et al. 1993; Ohyama et al. 2000; Tacconi et al. 1999). The HI absorbing gas samples a larger volume than the OH, and different structural components may contribute to the HI and molecular absorption component. However, the central OH and HI velocity gradients of about $0.25 \text{ km s}^{-1}\text{pc}^{-1}$ are surprisingly different from the velocity gradient of the CO $J = 2-1$ emission of $0.74 \text{ km s}^{-1}\text{pc}^{-1}$. Possibly the CO data also samples the higher gradients of the gas in the two disks.

The uniformly large line widths found in the HI and OH data confirm large-scale contributions to the central absorption. The large half-width values for HI and OH of 200 and 75 km s^{-1} are consistent with the stellar velocity dispersion peaking at 270 km s^{-1} close to the H_2 and CO $J = 2-1$ emission peaks (see Tecza et al. 2000). The large zero-intensity line widths of HI and OH confirm the presence of a disturbed and rather clumpy medium with multiple structures in the central region including the two nuclei (see also Beswick et al. 2001).

The OH–HI optical depth ratio in the central region suggests an OH/HI abundance ratio of 8.6×10^{-7} . This value is relatively high compared to other extragalactic absorption systems (see Baan et al. 1985), and would support the notion that the central region consists of enriched disk gas.

4.2. The two nuclei

Our data do not provide the detailed properties of the gas in the nuclear region and in the foreground. The HI and OH column densities suggest that the more obscured nucleus

N1 lies behind the less obscured northern nucleus. The path to N1 would then sample a more complex multiple absorption structure (see also Beswick et al. 2001). The total HI column density at N1 of $1.28 \times 10^{22} \text{ cm}^{-2}$ agrees with the column density estimated from X-ray nuclear emission (Komossa et al. 2003). In addition, the lower HI column at N2 of $1.01 \times 10^{22} \text{ cm}^{-2}$ also agrees with the X-ray column. The ratio of (integrated) OH and HI optical depths ranges between 0.25 at N1 to 0.32 at N2, which suggests lower enrichment at the nuclei relative to the central region.

Both nuclei have AGN characteristics in the radio and X-ray (Gallimore et al.; Beswick et al. 2001; Komossa et al. 2003). However, the extended radio continuum seen in the nuclear region forming the back-ground for the HI and OH absorption is associated with intense star-formation resulting from the close interaction of the galaxies (Genzel et al. 1998; Beswick et al. 2001). Extended radio structures of at least 1 kpc are commonly found in radio-quiet Seyferts and LINERs that do not follow the morphology of a galactic disk (Gallimore et al. 2006). Such extended structures result from nuclear outflows rather than starbursts and are likely to have a relatively luminous, compact radio source in the nucleus. Although NGC 6240 has evidence of a weak nuclear jet in the northern nucleus N2 (Gallimore & Beswick 2004), there is no evidence of strong AGN-related activity that could explain the total emission region covering a projected 7×4 kpc region that does not include the arc structure. It is more plausible that the AGNs in N1 and N2 have recently become active as a result of the interaction, and that the extended radio emission is due to distributed star-formation and the symmetric outflow triggered by the star-formation.

The distinct radio continuum region designated N3 is not necessarily a third nucleus, but is rather an area of enhanced (superposed) star-formation region in the interaction zone of the two galaxies and is currently embedded in the extended radio structure in the north.

4.3. The dynamics of NGC 6240

The nuclei N1 and N2 are separated by $1.575''$ corresponding to 793 pc. If the interacting galaxies were in the plane of the sky, they would be at a very different velocity and the nuclear regions would be coalesced and extremely confused. Since we see apparently distinct nuclear entities, they are more distant from each other and have only a projected distance of 793 pc. Considering that the highest HI and molecular column densities lie in between the nuclei and that the X-ray source in N1 shows the highest column density, it is most plausible that N1 lies behind N2. The small velocity difference suggests that the N1-N2 connecting axis has a small angle with the line-of-sight and the relative values of the velocities at N1 and

N2 suggest that the galaxies are just past transit.

The HI/OH systemic velocities at the nuclei can be used for a dynamical/orbital scenario for the nuclei projected on the sky. Given the relatively large beam, we find an HI estimate of 7235 and 7305 km s⁻¹ and an OH estimate of 7255 and 7370 km s⁻¹, which are nominally consistent with the higher resolution HI values of 7258 and 7440 km s⁻¹ (Beswick et al. 2001). These values are larger than the difference of stellar velocities of 50 km s⁻¹ (Tecza et al. 2000), but consistent with the H₂ (≈ 150 km s⁻¹), CO(2–1) (≈ 100 km s⁻¹), and Brackett γ emission data (Lira et al. 2002; Ohyama et al 2000; Tecza et al. 2000). We adopt the high-resolution HI estimate of the velocity difference for the nuclei $\delta V = 182$ km s⁻¹. The projected distance D_{obs} of the connecting line between the two galaxies is 1.575", which corresponds to a projected separation of 793 pc.

As an attempt at the dynamics of the close encounter, we assume a simple *edge-on circular orbit for two equal masses* M around the center of mass, and a (small) projection angle θ between our line of sight and the connecting line between the two nuclei. The description of the orbital motion of the system follows from: $\sin(\theta)^3 = 0.031 \delta V^2 G^{-1} M_n^{-1} D_{obs}$, where M_n is the combined dynamic mass of the nuclear region. The estimate of Tecza et al. (2000) of the stellar mass in each of the nuclei of about $2 \times 10^9 M_\odot$ gives a combined dynamic mass of the nuclei of $M_n = 1.2 \times 10^{10} M_\odot$ using the smaller velocity difference. The central gas concentration also constitutes a significant fraction of the dynamic mass, such that $M_{gas}(R \leq 470pc) \approx (2-4) \times 10^9 M_\odot \approx (0.3-0.7) M_{dyn}$ (Tacconi et al. 1999). For this reason, we adopt a dynamic mass for the nuclei of $M_n = 1.5 \times 10^{10} M_\odot$, which results in $\theta = 13.4^\circ$ (projection factor = 4.3), an orbital velocity of 392 km s⁻¹, and a distance between the nuclei of 3.42 kpc. The orbital period is about 27 Myr. This scenario gives a sufficiently large separation distance to ensure identifiable nuclear/galaxy characteristics at this well-advanced stage just before coalescence.

4.4. The two interacting galaxies

The OH and HI velocity field of the nuclear region is dominated by the large-scale organized motion of the accumulated gas structure. However, the detailed velocity pattern displayed in Figures 5a and 10a suggest the presence of large-scale velocity components associated with the interaction of the two galaxies. The analysis of the stellar velocity field in the southern galaxy suggests a northwest-southeast rotation ($i = 60^\circ$) at PA = -34° with $V_{rot} = 270 \pm 90$ km s⁻¹ (Tecza et al. 2000). The northern galaxy ($i = 33^\circ$) displays a southwest-northeast rotation at PA = 41° with $V_{rot} = 360 \pm 195$ km s⁻¹.

The HI and OH absorption in the northeast extension (Figs. 5a and 10a) shows a southwest-northeast rotation for the northern galaxy at $PA = 40\text{--}50^\circ$ with an HI gradient of 1.15 (or 0.75 for OH) $\text{km s}^{-1}\text{pc}^{-1}$ north of N2, which is consistent with a stellar gradient of 1.2 $\text{km s}^{-1}\text{pc}^{-1}$. However, the region south of N1 also shows evidence of a south-north rotation at 1.49 $\text{km s}^{-1}\text{pc}^{-1}$ for HI and 0.75 $\text{km s}^{-1}\text{pc}^{-1}$ for OH, and is associated with the large gas structure of the interaction. In addition, there is a weak low-velocity HI signature south of N1 down to 6900 km s^{-1} with the southwest-northeast gradient of 0.89 $\text{km s}^{-1}\text{pc}^{-1}$, which could constitute the motion of the southern galaxy. The absence of a clear velocity signature of the southern galaxy could easily result from the column density around N1. Furthermore, the region west-south-west of N1 is very perturbed by the outflow and shows evidence of components with velocities up to 7750 km s^{-1} .

4.5. The superwind outflow

The continuum structure extends from N1 and N2 in all directions, including to the northwest region and the radio arc. The western radio arc results from the shocked regions forming the boundaries of a symmetric superwind-driven outflow emanating from N1 (see Heckman et al. 1990), that is less prominent towards the east. In addition, there is a considerable extended radio emission resulting from distributed star-formation in the southwest and northeast regions. Besides the presence of two AGNs, the radio properties of the nuclear region suggest dominant starburst activity (Beswick et al. 2001; Gallimore & Beswick 2004). The K-band emission at both nuclei suggests a dominant population of red supergiants (Tecza et al. 2000). Recent X-ray data suggest that the outflow was indeed symmetric and that there are remnants on both sides of the nuclei.

The HI data shows a blue-shifted component along the line of sight extending to -300 km s^{-1} with respect to N1 (Fig. 4). Similarly there is a low velocity component in the OH data at -120 km s^{-1} (Fig. 9), which produces a wing on the 1667 MHz line (Fig. 7). Besides Ohyama et al. (2000) note a -250 km s^{-1} component in the H_2 emission. These blue-shifted features could represent line-of-sight outflows and shocks, which are driven into the denser nuclear ISM by the nuclear starburst and are associated with the superwind.

The HI and OH velocity and linewidth data west-south-west of N1 as well as the blue-shifted HI components at N1 clearly confirm that N1 is the origin of the outflows. The lifetime of the starburst has been estimated at $\approx 10 \text{ Myr}$ (Tecza et al. 2000), which is about 40% of the orbital period of 27 Myr derived above. The orbital motion may thus have resulted in smearing out the X-ray and radio emission regions. In addition, the difference of the emission strength of the northern and southern parts of the radio arc may also have

resulted from the "piling up" of emission in the forward direction, which confirms that N1 is moving north. The complicated OH and HI structures southwest of N1 are associated with the outflow into the western cavity and cover a large velocity range, with a mean of about 100 km s^{-1} below that of the systemic velocity of N1. There is (marginal) evidence of HI absorption components west-south-west of N1 reaching an extreme of 7750 km s^{-1} . Our HI data also displays continuous absorption against the base of the northern radio arc and against arc components W0, W2 and W4.

4.6. The extended absorption

The HI absorption is found across much of the extended radio emission, while the OH is found only in the central region of the source. The HI absorption shows complicated structures with a wide range of velocities and line widths, and relatively low column densities. Some of this material is associated with foreground dust lanes and ejected gas resulting from the interaction.

The extended radio emission in NGC 6240 is associated with the remnants of the two galaxies and the radio arcs resulting from the symmetric superwind outflows emanating from N1 and possibly N2. As discussed above, we find significant absorption and an HI velocity gradient of $1.0 \text{ km s}^{-1} \text{ pc}^{-1}$ in the NE region, which is associated with the remnant of the northern galaxy. In addition, there is an east-to-west gradient towards the NW region (at $\text{PA} = -50^\circ$), where we find the highest HI velocities in the system.

The column density map of Figure 6 displays widespread HI absorption in the large-scale structure of NGC 6240. Discrete absorption components with column densities in the range of $0.4 - 1.0 \times 10^{22} \text{ cm}^{-2}$ are found at the continuum component in the NW region and at the W0, W2, and W4 components of the arc structure. The velocities at these components, which are not associated with distinct components in the optical and $\text{H}\alpha$, suggest an increasing velocity towards the south.

The dominant absorption at W0 is caused by a north-south dust-lane passing in the foreground of the continuum structure with an estimated column density of $3.2 \times 10^{21} \text{ cm}^{-2}$. Images with various optical and X-ray instruments (Max et al. 2005; Komossa et al. 2003) show the clear presence of this north-south dust-lane that crosses the NW radio structure at W0 and accounts for an added column density. While the distributed HI in the NW region has a velocity of about 7500 km s^{-1} , the dust-lane has a systemic velocity of about 7270 km s^{-1} , which is close to that of N1. Furthermore, it has no clear velocity gradient because of its distance from the nuclei.

The radio continuum and X-ray images also display two extended structures S and SW of nucleus N1 (see Fig 1b; Komossa et al. 2003). It is found that a dust-lane structure towards the south divides these two structures. Only weak absorption has been seen against the continuum in this southern region.

4.7. The OH and H₂O emission

A narrow H₂O maser line has been detected towards the nuclear region of NGC 6240 at $V_{\text{lsr}} = 7565 \text{ km s}^{-1}$ located within 3 pc from the continuum peak at N1 (Hagiwara et al. 2003). The occurrence of an H₂O maser is rather unusual in a FIR dominated galaxy such as NGC 6240, which is more likely an OH Megamaser candidate. OH-MM UGC 05101 also hosts a weak H₂O maser towards the nuclear region (Zhang et al. 2005). The maser in NGC 6240 is redshifted about 300 km s^{-1} relative to the systemic velocity of N1, while high-velocity OH or HI gas has only been found in the northern region of the source (Figs. 3, 4, and 9). An association of the maser with the AGN could exist with shocked outflows, or jet-molecular cloud interactions in order to account for these discrepant velocities. Examples of other redshifted jet-related masers can be found in the elliptical NGC 1052 ($100\text{-}180 \text{ km s}^{-1}$; Claussen et al. 1998) and Mkn 348 (130 km s^{-1} ; Peck et al 2003). Alternatively, there could be either an association with infalling foreground gas to the nuclear region or with an active nucleus.

The shallow and multi-component Arecibo spectrum of OH in NGC 6240 has been interpreted on the basis of partial infilling of the absorption by emission (Baan et al. 1985). The asymmetries in the spectrum of Fig. 7 and the PV diagram Fig. 9 could indeed support this notion. While asymmetries suggest emission infilling at the velocity of N2, there is no evidence in the data for this. The bulk of the OH absorption shows an LTE line ratio. Only the western side of the central absorption shows non-LTE ratios that suggest infilling with emission at the low-velocity side of the 1667 MHz line at the velocity of N1. Non-LTE conditions could be caused by the FIR radiation field, which is dominant in NGC 6240 and has the right infrared colors for FIR pumping as in OH Megamasers (Baan 1989; Henkel and Wilson 1990). While there would be enough background radio continuum for this purpose in the N1 system, there is no discernable line emission.

5. Summary

The extended HI and OH absorption against the continuum structure has revealed more of the dynamic and evolutionary properties of the interacting system NGC 6240, and complementary evidence obtained at other wavelengths. The radio continuum structure and the associated absorption structure of NGC 6240 is in part the result of a superposition of the two galaxies and their constituents. In a simple dynamic model using HI systemic velocities, the northern galaxy with nucleus N2 would be located in front of the southern galaxy with nucleus N1, such that the N1-N2 connecting line would be foreshortened by a factor of 4.3. In this picture N1 would be expected to have the largest absorbing column density, while the central disks of the galaxies would be superposed between the two nuclei.

The radio continuum structure of $15'' \times 17''$ (7.6×8.6 kpc) peaks at the two nuclei of the interacting galaxies with hybrid starburst and AGN emission, and is surrounded by an extended structure associated with star-formation activity triggered by the interaction. A large-scale but incomplete loop structure on the western side of the source has been associated with a nuclear blowout and outflow from nucleus N1 of the southern galaxy, while traces of a similar structure can also be found at the eastern side of the source.

The HI absorption covers a contiguous $5'' \times 8''$ (2.7×4.2 kpc) region of the continuum structure and provides a large-scale view of the velocity field across this area. The peak of the HI absorption falls close to nucleus N1 in such a way that the HI column density at N1 is 1.26 times that of N2, and is in agreement with the estimates from X-ray observations.

OH absorption has been found only against the nuclear continuum and extends $2.5'' \times 2.0''$ (1.25×1.0 kpc). The largest column density of the OH absorption falls north of N1 and about halfway between N1 and N2, a fact that agrees with maps of other molecular emissions. The column densities at N1 and N2 are about 60% of that of the central gas structure.

The HI and OH velocity fields reveal parts of the velocity gradients of the two individual galaxies buried in the central region. Velocity gradients at various locations suggest gas motions resulting from the interaction of the two galaxies. In particular, the location of N1 and the region to the west displays blue-shifted (l.o.s.) outflow components, as well as structural components related to the sideways outflow into the western bubble. This evidence clearly confirms the nuclear activity at N1 as the origin of the outflows and the cause of the radio arc, which is consistent with the evidence from X-ray and $H\alpha$ data.

Distinct velocity components are found in the northern region and along the radio structure northwest of the nuclei. A foreground dust lane passes across the northwest radio loop structure. Absorption in more distant continuum components do not reveal a coherent

velocity pattern. The large width of the HI absorption line across the central part of the source confirms the violent dynamics of the system. The highest OH velocity widths are found at the central gas deposit, but they are significantly lower than those of HI and therefore less affected by the merger dynamics.

The central gas structure may result from a superposition of the disks of the two galaxies. There may also be accumulation of gas in the center of mass of the dynamic system. The central gas accumulation between the nuclei behaves as an independent structure with a velocity gradient proportional to the velocity difference of the two nuclei, and the gas appears locked into the motion of the system. The HI and OH velocity gradients for the central region are much smaller than that of CO(2–1), which may suggest that different observations detect distinctly different scale sizes within these structures.

The OH hyperfine ratio in the absorption region suggests mostly LTE conditions across the nuclear region, except in the western part of the central gas accumulation where non-LTE conditions are found. Non-LTE conditions may suggest that radiative far-infrared pumping actively reduces the absorption on the low-velocity side of the 1667 MHz OH line. No further OH maser emission has been found in the system.

WAB would like to thank Aubrey Haschick (formerly of Haystack Observatory) for constructive support during the early stages of this project.

REFERENCES

- Baan, W.A., Haschick, A.D., Buckley, D. & Schmelz, J.T. 1985, ApJ 293, 394
- Baan, W.A. 1989, ApJ 338, 804
- Beswick, R.J., Pedlar, A., Mundell, C.G. & Gallimore, J.F. 2001, MNRAS 325, 151
- Bland-Hawthorn, J., Wilson, A.S. & Tully, R.B. 1991, ApJ 371, L19
- Boller, Th. Keil, R. Hasinger, G., Costantini, E., Fujimoto, R., Anabuki, N., Lehmann, I. & Gallo, L. 2003, A&A 411, 63
- Claussen, M., Diamond, P.J., Braatz, J.A., Wilson, A.S. & Henkel, C. 1998, ApJL 500, L129
- Condon, J.J., et al. 1982, ApJ 252, 102
- Colbert, J.M.E., Wilson, A.S. & Bland-Hawthorn, J. 1994, ApJ 436, 89

- Fosbury, R.A.E. & Wall, J.V. 1979, MNRAS 189, 79
- Fried, J.W. & Schulz, H. 1983, A&A 118, 166
- Gallimore, J.F. & Beswick, R.J. 2004, AJ 127, 239
- Gallimore., J.F., Axon. D.J., O’Dea, C.P., Baum, S.A. & Pedlar, A. 2006, AJ 132, 546
- Genzel, R. et al. 1998, ApJ 498, 579
- Gerssen, J., van der Marel, R.P., Axon, D., Mihos, J.C., Hernquist, L. & Barnes, J.E 2004, AJ 127, 75
- Hagiwara, Y. 1998, PhD thesis, The Graduate University for Advanced Studies (GUfAS), Japan
- Hagiwara, Y., Diamond, P.J. & Myoshi, M. 2003, A&A 400, 457
- Iwasawa, K. & Comastri, A. 1998, MNRAS 297, 1219
- Joseph, R.D. & Wright, G.S. 1985, MNRAS 214, 87
- Heckman, T.M., Armus, L. & Miley, G.K 1990, ApJS 74, 833
- Henkel, C. & Wilson, T.L. 1990, A&A 229, 431
- Komossa, S., Burwitz, V., Hasinger, G., Predehl, P., Kaastra, J.S. & Ikebe, Y. 2003, ApJ 582, L15
- Lira, P., Ward, M., Zezas, A., et al. 2002, MNRAS 333, 709
- Max, C.E., Canalizo, G., Macintosh, B.A., Raschke, L., Whysong, D., Antonucci, R. & Schneider, G. 2005, ApJ 621, 738
- Nakanishi, K., Okumura, S.K., Hohno, K., Kawabe, R. & Nakagawa, T. 2005, PASJ 57, 575
- Ohyama, Y. et al 2000, PASJ 52, 563
- Peck, A.B., Henkel. C., Ulvestad, J.S., Brunthaler, A., Falcke, H., Elitzur, M., Menten, K.M. & Gallimore, J.F. 2003, ApJ 590, 149
- Sakamoto, K. Scoville, N.Z., Yun, M.S., Crosas, M., Genzel, R. & Tacconi, L.J. 1999, ApJ 514, 68
- Sanders, D.B., Soifer, B.T., Elias, J.T., Madore, B.F., Mathews, K., Neugebauer, G. & Scoville, N.Z. 1988, ApJ 470, 222

Scoville, N.Z., Yun, M.S. & Bryant, P.M. 1997, ApJ 484, 702

Tacconi, L.J., Genzel, R., Tecza, M., Gallimore, J.F., Downes, D. & Scoville, N.Z. 1999, ApJ 524, 732

Tecza, M., Genzel, R., Tacconi, L.J., Anders, S., Tacconi-Garman, L.E. & Thatte, N. 2000, ApJ 537, 690

van der Werf, P.P., Genzel, R., Krabbe, A., Bleitz, M., Lutz, D., Drapetz, S., Ward, M.J. & Forbes, D.A. et al. 1993, ApJ 405, 522

Zhang, J. S., Henkel, C., Kadler, M., Greenhill, L. J., Nagar, N., Wilson, A. S. & Braatz, J. A. 2006, A&A 450, 933

Table 1. Continuum Fluxes

Component	α (B1950)		δ (B1950)	1420 MHz		1667 MHz	
	h	m s		I_ν mJy b ⁻¹	S_ν mJy	I_ν mJy b ⁻¹	S_ν mJy
N1	16 50	27.84	02 28 57.5	108.8	225.9	55.7	88.2
N2 + N3	16 50	27.84	02 28 58.7			41.4	74.1
NW	16 50	25.70	02 29 00.2	6.03	-	3.3	6.3
W0	16 50	27.43	02 29 02.3	15.7	15.5	6.1	24.0
W1	16 50	27.18	02 29 02.6	6.65	-	3.4	6.4
W2	16 50	27.16	02 29 00.2	13.8	14.1	5.2	16.4
W3	16 50	26.92	02 28 56.6	11.1	-	4.4	14.4
W4	16 50	27.20	02 28 55.1	9.8	9.7	4.4	12.1
S	16 50	27.78	02 28 53.3	14.6	13.8	6.2	17.9
E1	16 50	28.20	02 28 57.1	1.5	-	-	-
NE	16 50	28.08	02 28 59.0	1.8	-	-	-
SE	16 50	27.90	02 28 55.1	4.0	5.7	-	-

Note. — The 21 cm and 18 cm continuum maps have an rms of respectively 0.30 and 0.27 mJy beam⁻¹.

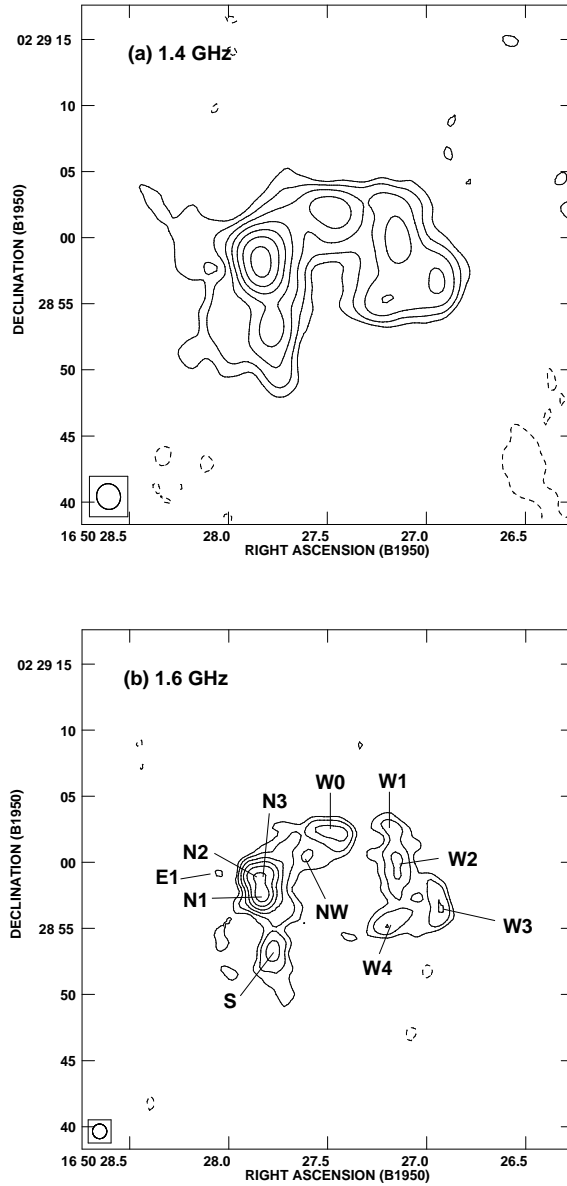


Fig. 1.— Continuum structure at L-band towards NGC 6240. *Upper panel:* the 1420 MHz continuum emission with contour levels of -1 and 1 to 128 by factors of two times 1.2 mJy beam⁻¹. The peak in the map is 108.8 mJy beam⁻¹. *Lower panel:* the 1666 MHz continuum emission with contour levels of -1 and 1 to 64 by factors of two times 1.1 mJy beam⁻¹. The peak in the map is 55.7 mJy beam⁻¹. Labelling of components according to the nomenclature of Colbert et al. (1994).

Table 2. HI and OH Absorption Parameters

Component	V(HI) ^a (km/s)	ΔV^b (km/s)	τ_{HI}	$\int \tau_{HI} dv$ (km/s)	N_H^c (cm^{-2})	V(OH67) ^a (km/s)	ΔV^b (km/s)	τ_{OH67}	$\int \tau_{OH} dv$ (km/s)	N_{OH67}^d (cm^{-2})
Nucleus N1	7295	909	0.15	70.4±0.7	1.28 (22)	7243	295	0.038	1.39±0.1	6.55 (15)
Central Peak	7295	913	0.12	70.4±0.7	1.28 (22)	7274	406	0.063	2.29±0.2	1.1 (16)
Nucleus N2	7339	870	0.11	55.5±0.5	1.01 (22)	7363	406	0.035	1.28±0.1	6.03 (15)
NE corner	7600	303	0.52	25.6±1.5	4.67 (21)	-	-	-	-	-
NW comp	7513	606	0.07	34.2±1.3	6.23 (21)	-	-	-	-	-
Dust lane	7270	800	0.05	51.7±1.2	9.42 (21)	-	-	-	-	-
E1 comp	7530	380	0.04	46.8±1.3	8.55 (21)	-	-	-	-	-
W2 comp	7034	217	0.04	21.4±1.5	3.90 (21)	-	-	-	-	-
W4 comp	7687	390	0.07	42.7±1.3	7.80 (21)	-	-	-	-	-

^aPeak values.

^bFull width zero-intensity values.

^cAssumed $T_S=100$ K for HI.

^dAssumed $T_{ex}=20$ K for OH.

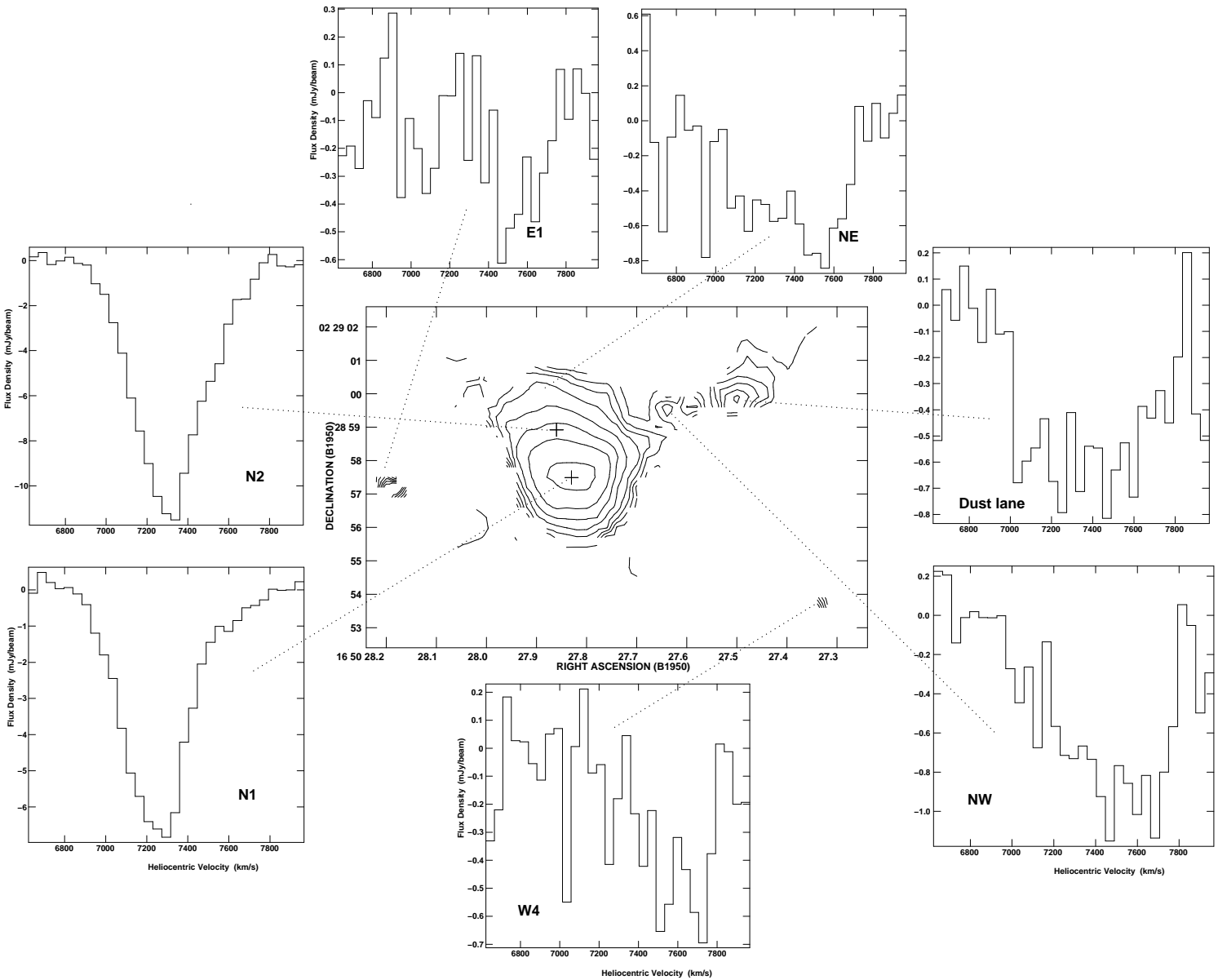


Fig. 2.— Spectral signatures of the HI absorption in NGC 6240. The zeroth moment map of integrated HI absorption is presented in the central frame and is similar to Figure 6. The spectra at seven locations have velocity tick marks of 6800 to 7800 km s^{-1} . We note that the significance of the spectral profiles is low at some locations in the column density maps.

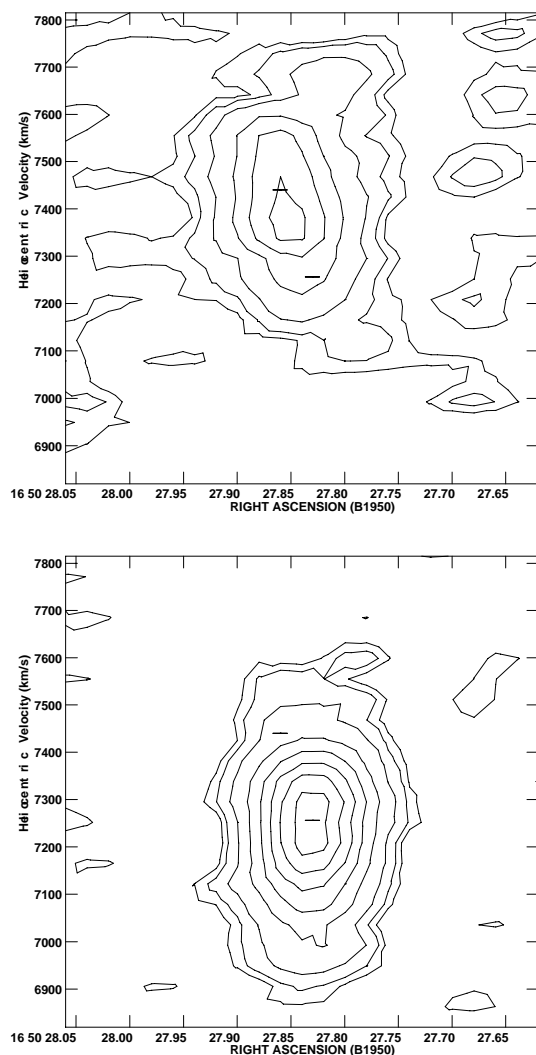


Fig. 3.— The HI velocity-position diagrams in the nuclear region for two declinations. The systemic velocities of N1 and N2 are 7258 and 7440 km s^{-1} . *Upper diagram:* Close to nucleus N2 at declination $02\ 28\ 59.9$. *Lower diagram:* Close to nucleus N1 at declination $02\ 28\ 57.2$. For an rms of 0.45 mJy beam^{-1} , the contour levels are at $0.5, 1, 2, 4, 6, 8, 10, 12, 14, 16$ mJy beam^{-1} . The declination-velocity locations of the two nuclei have been marked in the diagrams. Features at the lowest contours have a marginal significance.

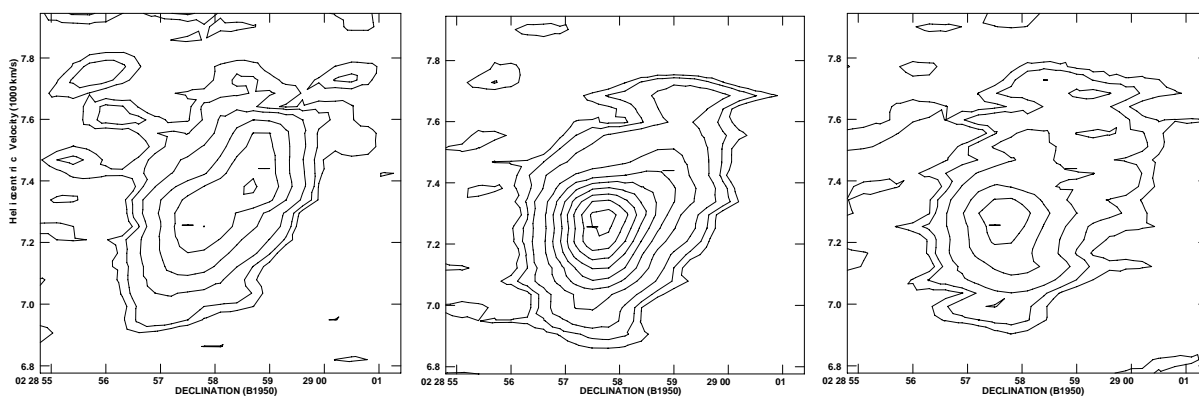


Fig. 4.— The HI velocity-position diagrams in the nuclear region for three RA values. The systemic velocities of N1 and N2 are 7258 and 7440 km s^{-1} . *Left diagram:* Just east of nucleus N2 at $\text{RA} = 16\ 50\ 27.88$. *Middle diagram:* Just west of nucleus N1 at $\text{RA} = 16\ 50\ 27.82$. *Right diagram:* West of nucleus N1 and N2 at $\text{RA} = 16\ 50\ 27.78$. For an rms in these maps of 0.45 mJy beam^{-1} , the contour levels are at $0.5, 1, 2, 4, 6, 8, 10, 12, 14, 16$ mJy beam^{-1} . The declination-velocity locations of the two nuclei have been marked in the diagrams. Features at the lowest contours have a marginal significance.

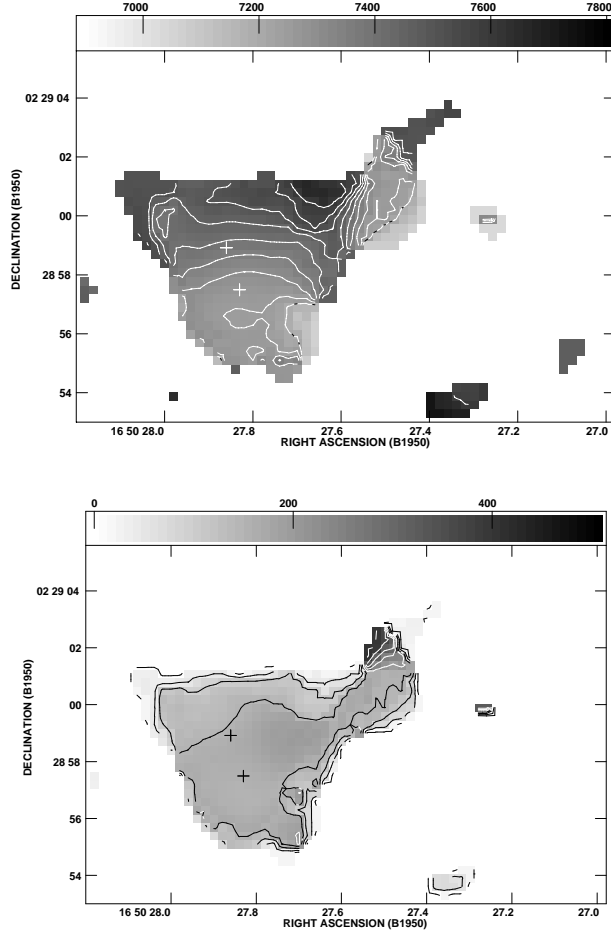


Fig. 5.— HI velocity moment maps. Positions of N1 and N2 are marked by crosses. *Upper diagram*: HI 1st moment map. Contours are plotted at 7200, 7250, 7300, 7350, 7400, 7450, 7500, 7550, and 7600 km s⁻¹. The grey-scale is from 6900 to 7800 km s⁻¹. *Lower diagram*: HI 2nd moment map, showing HI velocity dispersion. Contours are plotted at 10, 50, 100 to 500 by 50 km s⁻¹. The grey-scale starts at 0 km s⁻¹ and ends at 500 km s⁻¹. The central region has velocity half-widths greater than 150 km s⁻¹.

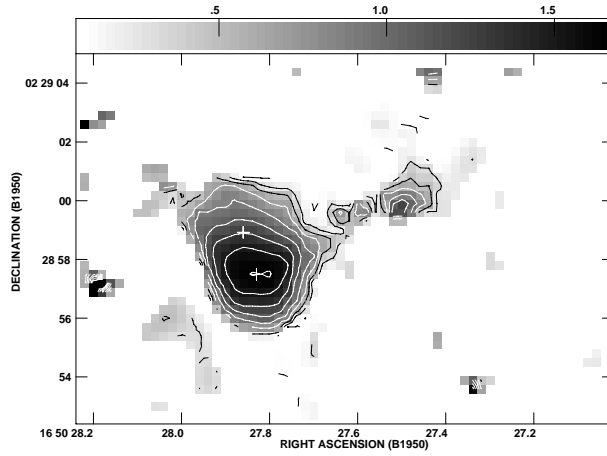


Fig. 6.— HI absorption column density map. Contours for N_{H} are 0.1, 0.3, 0.5, 0.7, 0.9, 1.1, 1.3, 1.5, and 1.64 and grey scale from 0.1 to 1.64 in units of $7.78 \times 10^{21} \text{ cm}^{-2}$ assuming $T_S = 100 \text{ K}$.

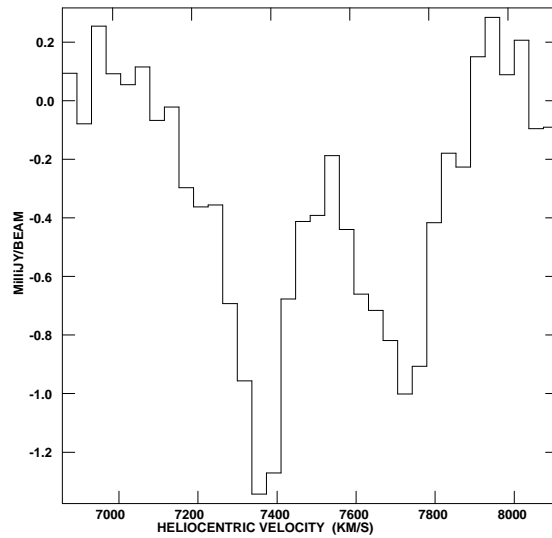


Fig. 7.— Integrated spectrum of OH absorption taken across both nuclei with the 1667 MHz (left) and the 1665 MHz (right at $+351 \text{ km s}^{-1}$). The velocity axis of the spectrum is in the rest frame of the 1667 MHz line.

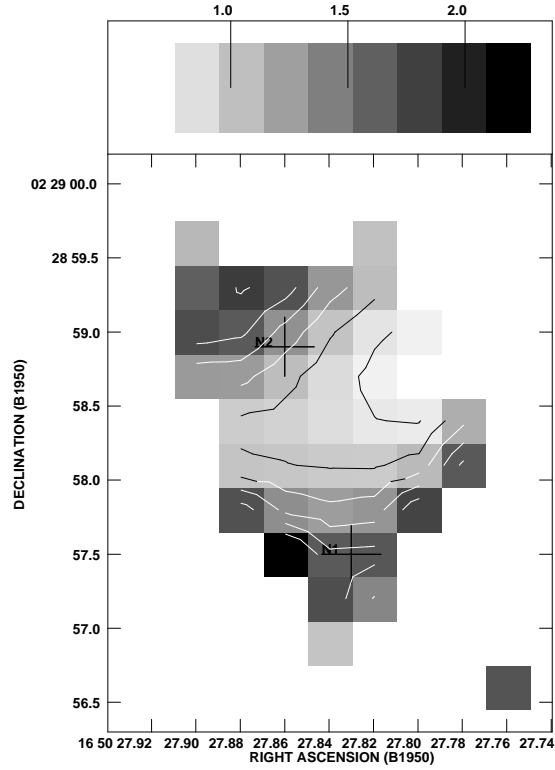


Fig. 8.— The hyperfine line ratio of the 1667 and 1665 MHz absorption lines across the nuclear region. The location of the two nuclei are indicated in the diagram. The contour levels are 0.8–1.8 with intervals of 0.2. The lowest contour of 0.8 is at the west side of the central region and subsequent contours are increasingly further out towards the two nuclei. Values of 1.6 are found at N1 and 1.2 at N2. The highest optically–thin ratio of 1.8 is found north of N1, while south of N1 the ratio decreases again to 1.4.

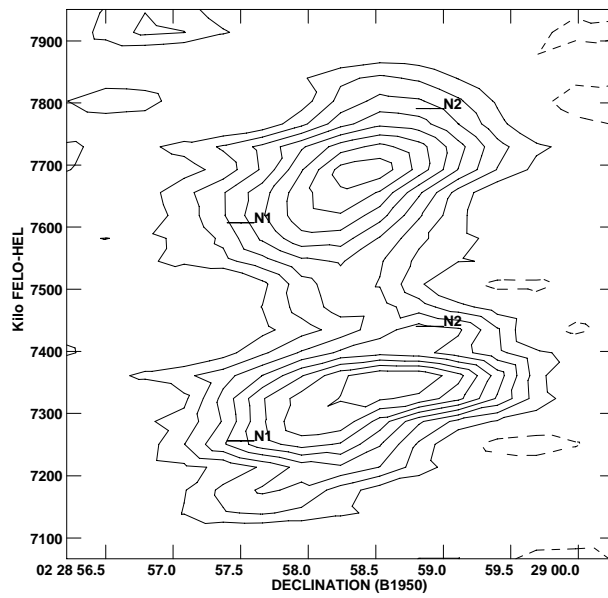


Fig. 9.— Position-velocity map of the 1667/1665 MHz OH absorption along P.A.=20° along the N1–N2 line. The spectrum has been inverted for presentation. The RA - velocity position of each of the nuclei has been indicated in the diagram. For an rms of $0.29 \text{ mJy beam}^{-1}$, the contours are plotted at $-1, 1, 2, 3, 4, 5, 6, 7,$ and $8 \times 0.55 \text{ mJy beam}^{-1}$. Features at the lowest contour have marginal significance.

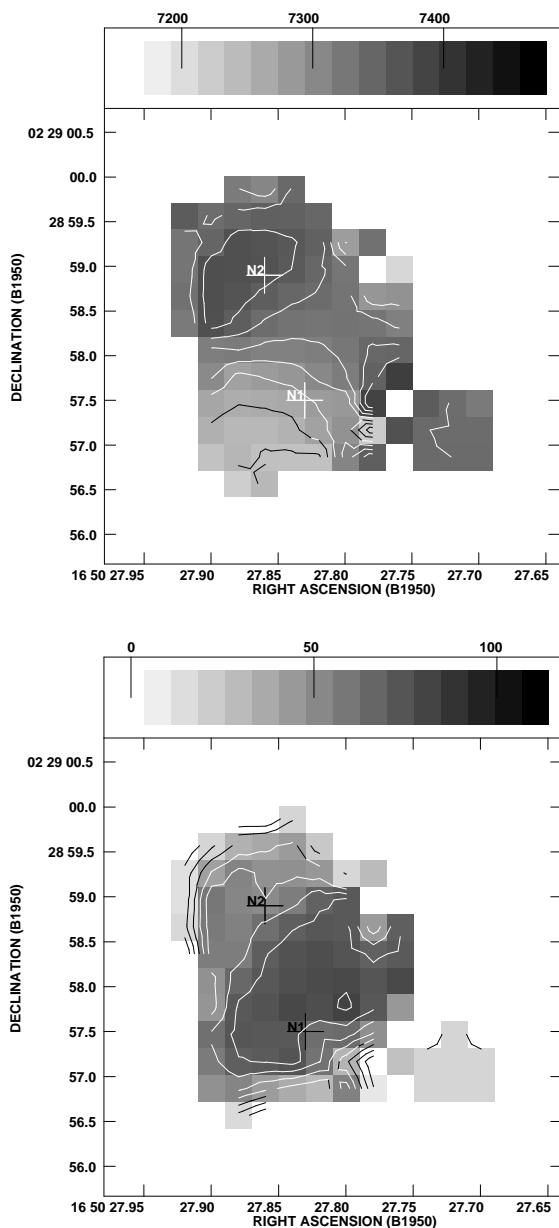


Fig. 10.— First and second moment maps of the OH 1667 MHz line. The locations of the twin-nuclei are marked by crosses. *Upper diagram* First moment: The line velocity contours superposed on the grey-scale are spaced linearly by 20 km s⁻¹ beginning at 7240 km s⁻¹ and ending at 7360 km s⁻¹. The peak value is 7393 km s⁻¹ and the values at N1 and N2 are 7275 and 7370 km s⁻¹. Grey-scale range is from 7150 km s⁻¹ to 7400 km s⁻¹. *Lower diagram* Second moment: The line width contours are at 20 to 80 km s⁻¹ with increments of 10 km s⁻¹. The central region has a line width of 80+ km s⁻¹.

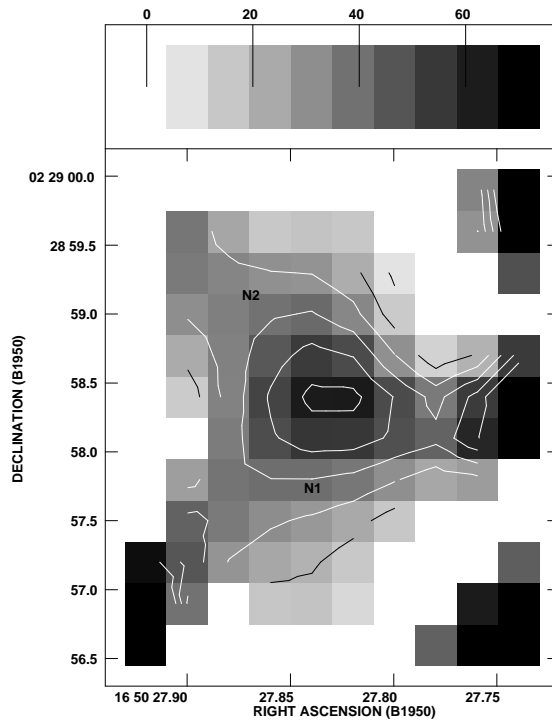


Fig. 11.— OH column density map of 1667 MHz. The integrated column density contours are 1, 2, 4, 6, 8, 10, and 12 times $8.62 \times 10^{14} \text{ cm}^{-2}$ using an excitation temperature of $T_{ex} = 20 \text{ K}$. The grey scale displays the corresponding optical depth on a scale of 0 to 0.06. The peak optical depth is 0.063 with a column density of $1.08 \times 10^{16} \text{ cm}^{-1}$.